Epitaxial Growth and Processing of Compound Semiconductors

Academic and Research Staff
Professor Leslie A. Kolodziejski, Dr. Gale S. Petrich

Alexei A. Erchak, Elisabeth M. Koontz, Aleksandra Markina and Sean C. Warnick

Undergraduate Student
Solomon Assefa

Technical and Support Staff
Diane W. Hagopian and Donna L. Gale

Keywords: heteroepitaxy, compound semiconductors, electronic materials, III-V, optoelectronic devices

I. Introduction

The emphasis of this research program is the epitaxial growth and processing of III-V compound semiconductors. The epitaxial growth of the heterostructures is performed in the chemical beam epitaxy laboratory. The laboratory consists of two gaseous source epitaxy reactors interconnected to several smaller chambers, which are used for sample introduction and *in-situ* surface analysis. Such a multichamber epitaxy system allows heterostructures to be fabricated within a continuous ultrahigh vacuum environment. The III-V gas source molecular beam epitaxy (GSMBE) reactor is equipped with (1) solid elemental sources of Ga, In, Al, Si and Be, (2) gaseous hydride sources of arsenic and phosphorus, (3) an atomic hydrogen source to remove the sample's native surface oxide prior to growth and (4) an *in situ* spectroscopic ellipsometer to characterize the epilayer during growth.

In the following sections, the status of the various III-V-based projects will be discussed. The III-V GSMBE system is utilized for the development of (In,Ga)(As,P)-based optical devices for all-optical communication networks and the fabrication of GaAs-based devices implementing one- and two-dimensional photonic bandgap crystals within their structure.

II. Development of Components for Ultrafast All-Optical Communication Networks

Sponsors
U. S. Air Force Office of Scientific Research
Multidisciplinary Research Grant F49620-96-1-0126 (OSP 64450)
MIT Lincoln Laboratory
Contract Number (OSP 64320, OSP 67357)

Keywords: (In,Ga)(As,P), GSMBE, Photonic Devices, Mode-locked Lasers, Saturable Absorber, Patterned Surface Overgrowth

The need for ultrafast (100 Gbits/sec) all-optical communication networks is intensifying as the amount of data-containing communication traffic continues to grow at an exorbitant rate. Although wavelength division multiplexed (WDM) systems are in the process of being implemented, aggregate data rates may be limited by electronic signal processing speeds at the originating and terminating ends of the fiber optic networks. The ability to move away from electronic processing and towards all-optical processing of the network-level data is attractive for the realization of high speed communication networks due to simplicity of integration and possible elimination of optoelectronic conversion.

In order to eliminate electronic processing on the network level, all-optical processing components must transfer, store, and rate-convert all data to and from the data rate of the source (i.e. a computer) to the network data transmission rate. Thus, components such as passive wavelength-selective routers and all-optical switching mechanisms need to be implemented. Additionally, ultrafast (femtosecond) optical sources are required to provide the high bit data and clock rates for the networks.

II.A Gas Source Molecular Beam Epitaxial Overgrowth of Rectangular-Patterned In(Ga,As)P Surfaces

Project Staff:

Prof. Leslie A. Kolodziejski, Prof. Henry I. Smith, Dr. Mark S. Goorsky*, Dr. Gale S. Petrich, Elisabeth Marley Koontz, and Michael H. Lim

* Department of Materials Science and Engineering, UCLA, Los Angeles, CA 90095

The ability to epitaxially deposit material on patterned surfaces is a key fabrication step for the realization of many optical sources, optoelectronic integrated circuits, and optical filters. InP-based communication-oriented devices, as well as reduced-dimensionality heterostructures such as quantum wires and quantum boxes, rely on the successful overgrowth of periodic-patterned corrugations. The primary motivation for the overgrowth of corrugated surfaces stems from the requirement of creating a variation in the refractive index for photonic or optoelectronic devices such as distributed feedback (DFB) lasers, Bragg-resonant filters [1,2,3], and resonant grating waveguides [4]. Mastery of the overgrowth process, specifically the minimization of overgrowth-generated defects, increases design flexibility by allowing the placement of the corrugation anywhere within the device, and also furthers the realization of quantum wire-based devices.

The investigation into the overgrowth of rectangular-patterned gratings is motivated by the need to fully preserve the as-fabricated grating profile in order to realize devices such as Bragg-resonant channel dropping filters [3]. The strong rectangular-defined index contrast establishes the reflectivity of the Bragg resonators; alteration of the profile from a rectangular shape severely diminishes the filter performance, rendering it virtually useless for high density WDM applications [5]. To date, the majority of rectangular-like profile overgrowth studies have been applied to larger-dimensioned structures, such as selective-area growth for device integration (e.g. [6,7]) or for buried heterostructure devices (e.g. [8,9,10,11,12]). In general, rectangular profiles are fabricated via reactive ion etching (RIE) which introduces the issue of crystallographic damage of the material in proximity to the etched surface [13,14]. The fabricated profiles typically contain vertical sidewall facets of either $(0\,\bar{1}\,\bar{1})$ or $(0\,\bar{1}\,1)$. The vertical sidewalls are different from the {*h*11} variety of sawtooth-patterned gratings in that both Group III and Group V atoms are present on the surface and only single dangling bonds are exposed; thus, the incorporation of adatoms and associated migration lengths on the sidewalls are expected to differ from that of sawtooth-patterned grating overgrowth.

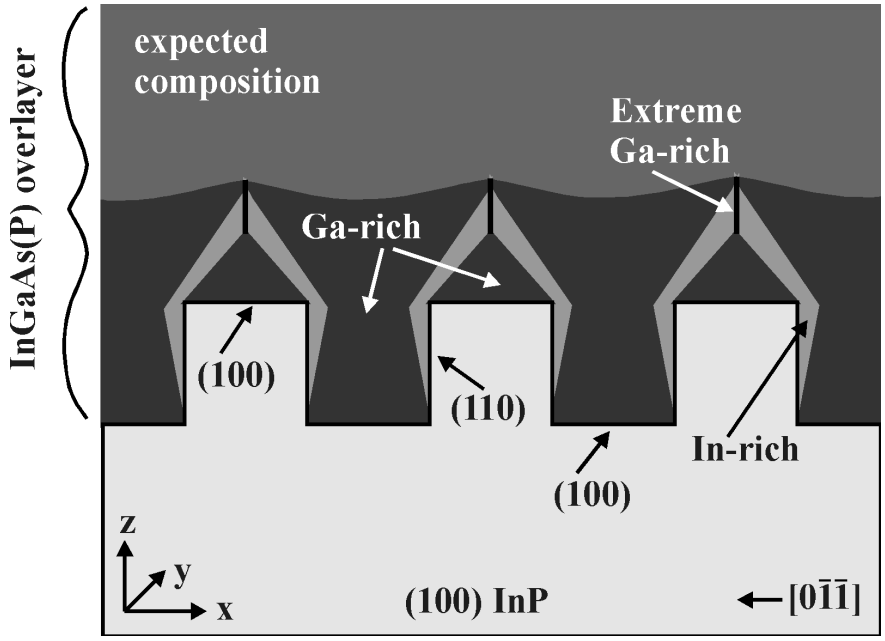

Figure 1) Schematic illustration of the overgrowth process of InGaAs(P) on rectangular-patterned (100) InP surfaces.

To illustrate the overgrowth process, a preliminary model for the (In,Ga)(As,P) overgrowth of rectangular-patterned surfaces has been developed and is depicted in Figure 1. From marker layer overgrowth studies by Izrael, *et al* of InP rectangular-patterned surfaces [15], as the overlayer material is deposited in the trenches, facets begin to develop between the (100) growth front (dictated by the trench base) and the (110) grating tooth sidewalls; these facets appear to be similar to {*h*11} facets, and will most likely not be preferred incorporation sites for Ga adatoms. Thus the Ga adatoms will tend to migrate towards the center of the trench or the top of the grating teeth. (Note, the model in Figure 1 assumes the preservation

of the rectangular grating profile and (100) trench and tooth surfaces.) Although in reference to GaAs/AlGaAs quantum wire formation, the analytical model developed by Biasiol and Kapon also predicts the formation of {*h*11}-type facets within (100) grating grooves [16]. Similar to the results described for sawtooth-patterned overgrowth, a 'triangular region' of Ga-rich material is expected to develop on top of the grating teeth (as a result of deposition on a mesa-like profile). The localization of Ga adatoms will result in Ga-deficient regions that correspond to the non-(100) growth fronts. The occurrence of an extremely Ga-rich column above the 'triangular region' would also not be unexpected, and the thickness would depend on the planarization rate of the Ga-rich region within the grating trenches. As the surface of the overlayer begins to planarize, the Ga adatoms will incorporate more readily on surfaces that approach a (100) orientation, and the overlayer composition will become the same as that of a planar epilayer. As with sawtooth-patterned overgrowth, the thickness required to achieve a planar overlayer will decrease as the concentration of Ga and As is decreased; this is evident from a cusped surface of a ~200 nm $In_{(1-x)}Ga_xAs$ (x~0.47) overlayer compared to a planar surface of a ~210 nm $In_{(1-x)}Ga_xAs_yP_{(1-y)}$ (x~0.1, y~0.29) overlayer, both deposited on preserved rectangular-patterned InP substrates.

Given the model in Figure 1, the existence of compositional modulation within an $In_{(1-x)}Ga_xAs_yP_{(1-y)}$ (x~0.1, y~0.29) overlayer deposited on an InP rectangular corrugation is probable. Room temperature photoluminescence (PL) measurements disclose a difference in the emission wavelength between the planar monitor sample (λ~1.095 μm) and the grating overgrowth sample (λ~1.083 μm). Furthermore, from triple axis x-ray diffraction (TAD)-generated {422} reciprocal space maps (RSMs) (see Figure 2), the large range of Δq_x (-11 $\mu m^{-1} < \Delta q_x <$ 8 μm^{-1}) as well as the range of Δq_z (~ -34 $\mu m^{-1} < \Delta q_z <$~-20 μm^{-1}) of the InGaAsP overlayer may be suggestive of compositional modulation and/or variation in a_x and a_z (see Figure 1 for the definition of coordinates). However, from work reported for sawtooth-patterned overgrowth, the small amount of Ga and As within the InGaAsP (x~0.1, y~0.29) overlayer would result in minor compositional modulation. Also, with such a thin overlayer (~210 nm), the grating region (~80 nm) occupies roughly half the total overlayer thickness. Thus, any variation in lattice parameters (not necessarily expected to be constant throughout the grating region), due to strain accommodation in the grating region, would comprise a large portion of the overlayer and be detectable via asymmetric x-ray diffraction measurements.

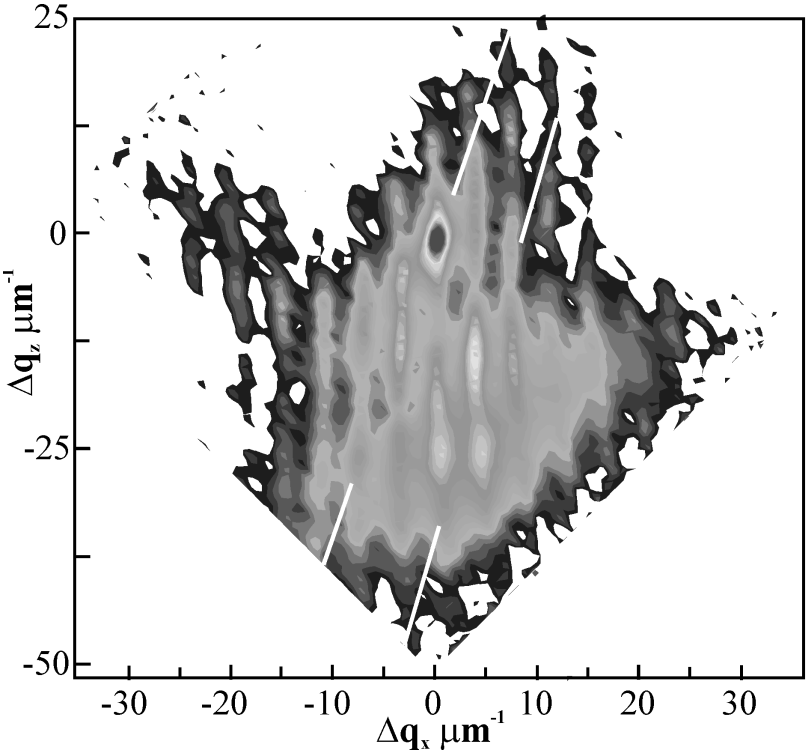

Figure 2) Asymmetric {422} glancing exit reciprocal space map obtained from the overgrowth of $In_{(1-x)}Ga_xAs_yP_{(1-y)}$ (x~0.1, y~0.29) on rectangular-patterned InP substrates. $\Delta q_x > 0$ corresponds to an increase in a_x. The intensity scale is 1-10^4.

Initial analysis of the PL and TAD data suggests a difference in the InGaAsP overlayer composition from that measured from the planar monitor sample. Using the observed PL emission wavelength for the InGaAsP bandgap, (400) high resolution dynamical x-ray diffraction simulations indicate a decrease in mole fraction of both Ga and As for the overlayer. However, a decrease in the Ga mole fraction is not expected if the overgrowth model is assumed since the Ga-deficient region should be small due to the small concentration of Ga and As atoms in the overlayer. Consequently, the difference in strain observed in the overgrowth sample (ε_z~3.6x10^{-3}) relative to the planar monitor (ε_z~4.5x10^{-3}), albeit small, can not be overlooked. From Figure 1, the changes in strain of the overlayer, with respect to the planar $In_{(1-x)}Ga_xAs_yP_{(1-y)}$ (x~0.1, y~0.29) epilayer, are calculated to be $\Delta\varepsilon_x$~5.2x10^{-4} and $\Delta\varepsilon_z$~-9.0x10^{-4} (from (422) RSMs parallel to the rectangular corrugation, a_y is equal to the in-plane lattice constant of InP, so $\Delta\varepsilon_y$~0). Thus, the overlayer material above the grating region experiences an orthorhombic lattice distortion. Taking into account the reduced strain in both a_z and a_x, calculations of the bandgap [17,18] for a strained $In_{(1-x)}Ga_xAs_yP_{(1-y)}$ (x~0.1, y~0.29) overlayer indicate that room temperature PL emission is expected at λ~1.092 μm. Considering the average change in orthorhombic strain (with respect to the planar epilayer) of the quaternary material within the grating trenches, bandgap calculations suggest a 300K PL emission of λ~1.083 μm. The room temperature PL spectrum exhibits a single broad feature peaked at λ~1.083 μm, and clearly encompasses emission originating from the quaternary in both the grating trenches and beyond the grating region. (Similar modifications to the bandgap of InGaAs/GaAs buried quantum wires have also been observed [18].) Therefore, the orthorhombic lattice distortion and change in bandgap of the quaternary material may be

attributed to strain in the overlayer caused by the InP grating, rather than to compositional modulation. Stress exerted on the overlayer above the grating region is not surprising since the total overlayer thickness is only roughly twice the thickness of the grating region. As the overlayer thickness is increased, such that the grating region is only a fraction of the overlayer thickness, the orthorhombic distortion of the overlayer will decrease; e.g. no strain modification of the overlayer above the grating region is observed in structures with~1 μm of InP deposited on InGaAsP gratings. Strain variation on the order of 10^{-3} and less, and bandgap modifications on the order of 10 meV and lower (with respect to the planar sample), due to the orthorhombic strain of the InGaAsP overlayer are minor alterations and will most likely not have a pronounced effect on devices incorporating buried rectangular-patterned gratings.

II.B Development of Semiconductor Saturable Absorber Mirrors for Mode-locked Fiber Lasers

Project Staff:

Prof. Leslie A. Kolodziejski, Prof. Erich P. Ippen, Dr. Franz X. Kärtner,* Dr. David J. Jones,** Dr. Marcus Joschko,*** Dr. Patrick Langlois,**** Elisabeth Marley Koontz, Erik R. Thoen, Thomas Schibli*

* currently with Universität Karlsruhe, Kaiserstrasse 12, D-76128 Karlsruhe, Germany
** currently with JILA, University of Colorado and National Institute of Science and Technology, Boulder, CO 80309
*** no longer affiliated with MIT
**** currently with Nortel Networks, Ottawa Canada K1Y 4H7

Generation of ultrashort pulses is directly applicable not only to optical communication networks, but also to investigation of ultrafast nonlinear processes [19] and optical imaging of biological tissue (e.g. optical coherence tomography [20]). Passive mode-locking techniques for the generation of ultra-short pulse trains are preferred over active techniques due to the ease of incorporation of passive devices into various laser cavities. A passive mode-locking device, the semiconductor saturable absorber mirror, has recently been used to mode-lock a wide range of laser cavities [i.e. 21,22,23,24,25]. Pulses result from the phase-locking (via the loss mechanism of the saturable absorber) of the multiple lasing modes supported in continuous-wave laser operation. The absorber becomes saturated at high intensities, thus allowing the majority of the cavity energy to pass through the absorber to the mirror, where it is reflected back into the laser cavity. At low intensities, the absorber is not saturated, and absorbs all incident energy, effectively removing it from the laser cavity. As a result of the absorber behavior, the supported modes are forced to operate at the same phase condition in an effort to minimize intra-cavity loss, resulting in the generation of pulses.

Although semiconductor saturable absorber mirrors have been employed for mode-locking in a wide variety of laser cavities, it is crucial to design a saturable absorber mirror for each specific application. The differing loss, gain spectrum, internal cavity power, etc, of each laser necessitates slightly different absorber characteristics. The laser cavity for which the saturable absorber mirrors are currently being designed is a fiber laser cavity with an Er/Yb codoped waveguide amplifier. This laser cavity is extremely attractive because it is theoretically scalable to very short cavity lengths, such that the entire cavity consists of the waveguide amplifier with a high reflector and saturable absorber mirror both butt-coupled, with index-

matching fluid, to the waveguide facets. (For this type of arrangement, the laser diode amplifier pump will reside outside of the laser cavity.) An ultrashort laser cavity of this type is particularly attractive for use in all-optical high-speed communication networks. The compactness of the cavity is not only beneficial from a size perspective (5.2 cm), but also from a repetition rate perspective; such a small mode-locked cavity would be expected to generate pulses at repetition rates of ~2 GHz.

The semiconductor saturable absorber mirror structures that are currently being developed are deposited via gas source molecular beam epitaxy (GSMBE). The GaAs/AlAs distributed Bragg reflector (DBR) is first deposited and analyzed via transmission measurements. The absorber region (InP-based) is then deposited, utilizing a low temperature atomic hydrogen oxide removal process to prepare the DBR surface. Photoluminescence (both 10K and 300K) and transmission measurements are performed to characterize the saturable absorber mirrors. Thus far, the semiconductor saturable absorber mirrors have been characterized under conditions similar to those within a mode-locked laser cavity via pump-probe and energy fluence measurements [26,27,28]. The semiconductor saturable absorber mirrors have also been used to mode-lock both fiber lasers incorporating an Er/Yb codoped waveguide amplifier [29,30] and Er/Yb codoped fiber amplifier.

The saturable absorber mirror used in the fiber laser with an Er/Yb codoped waveguide amplifier contains a 22 pair AlAs/GaAs DBR producing a reflectivity greater than 99%, centered at λ~1.55 μm. The InP-based absorber consists of a ~100 nm thick InGaAs absorber (λ~1.58 μm) centered within an InP half-wave layer. The absorption characteristics of the structure are enhanced via the deposition of an antireflection dielectric coating.

A detailed description of the absorber mirror analysis and the performance of mode-locked fiber lasers implementing these saturable absorber mirrors may be found in Professor Ippen's section of the Progress Report.

II.C Development of Semiconductor Optical Amplifiers for All-Optical Signal Processing

Project Staff:
Professor Leslie A. Kolodziejski, Dr. Katherine L. Hall*, Dr. Mark Kuznetsov*, Dr. Joseph Donnelly*, Dr. Gale S. Petrich, Elisabeth M. Koontz and Aleksandra Markina

* MIT Lincoln Laboratory

Sponsor
MIT Lincoln Laboratory
Contract Number (OSP 67357)

Semiconductor Optical Amplifiers (SOAs) are an attractive alternative to silica fiber amplifiers. Advantages of SOAs include their smaller size, larger bandwidth, and ease with which SOAs can be incorporated into optoelectronic integrated circuits [31]. SOAs have a wide range of uses in communication systems such as optical amplification, all-optical switching, optical demultiplexing, wavelength conversion, clock recovery, and dispersion compensation [32,33].

One of the main advantages of a heterostructure design for a SOA is that the thickness of an active layer can be dramatically reduced. A smaller active region thickness allows an amplifier to demonstrate a substantial gain even at very low injected current densities. The compositional profile is designed to confine carriers to the active region, which is much shorter than the carriers' diffusion length. In addition, the active layer is designed to have a larger index of refraction than that of the cladding layers, causing the confinement of light to an active region with a thickness smaller than the wavelength of light. Thus, the active region essentially represents an optical waveguide. To operate a SOA as a broadband single-pass device, its facets must be coated with an antireflective coating to avoid the creation of resonator modes [31].

This project aims to develop, fabricate, and characterize an InGaAsP/InP SOA structure. The chosen material system, (In,Ga)(As,P), offers a range of bandgap energies compatible with all-optical fiber networks and can be grown by gas source molecular beam epitaxy (GSMBE) on InP substrates. GSMBE growth is effectively used to achieve atomically abrupt doping and refractive index profiles. In the current design, an active $In_{0.56}Ga_{0.44}As_{0.93}P_{0.07}$ layer and $In_{0.91}Ga_{0.09}As_{0.2}P_{0.8}$ cladding layers are surrounded by dopant-graded InP layers. In order to make the device polarization insensitive, the quaternary materials are closely lattice matched to InP [34]. The active layer has a bandgap that corresponds to a wavelength λ=1.57 μm, catering to a λ=1.55 μm lightwave communication system.

As a first step in preparation for the fabrication of the SOA structure, GSMBE growth of quaternary layers and doped InP layers were performed for calibration purposes. For each quaternary layer, high-resolution double-axis x-ray diffraction was used to monitor the perpendicular lattice constant. Photoluminescence was performed to measure the bandgap of the quaternary materials. The composition of each quaternary film is determined from its measured bandgap and perpendicular lattice constant. Dopant concentrations of Si- and Be-doped InP epilayers are found through Hall Effect measurements of carrier mobility and sheet resistivity.

II. D Publications

Koontz, E. M., G. D. U'Ren, M. H. Lim, L. A. Kolodziejski, M. S. Goorsky, G. S. Petrich, and Henry I. Smith, "Overgrowth of (In,Ga)(As,P) on Rectangular-Patterned Surfaces Using Gas Source Molecular Beam Epitaxy." J. Cryst. Growth, 198/199: 1104-1110 (1999).

Koontz, E.M., G. S. Petrich, L. A. Kolodziejski, and M. S. Goorsky, "Overgrowth of Submicron-Patterned Surfaces for Buried Index Contrast Devices." Semiconductor Science and Technology, Forthcoming.

Thoen, E.R., E. M. Koontz, M. Joschko, P. Langlois, T. R. Schibli, F. X. Kartner, E. P. Ippen, and L. A. Kolodziejski, "Two-Photon Absorption in Semiconductor Saturable Absorber Mirrors." Appl. Phys. Lett., 74(26): 3927-3929 (1999).

Langlois, P., M. Joschko, E. R. Thoen, E. M. Koontz, F. X. Kartner, E. P. Ippen, and L. A. Kolodziejski, "High Fluence Ultrafast Dynamics of Semiconductor Saturable Absorber Mirrors." Appl. Phys. Lett., 75(24): 3841-3843 (1999).

Thoen, E.R., E. M. Koontz, D. J. Jones, D. Barbier, F. X. Kartner, E. P. Ippen, and L. A. Kolodziejski, "Erbium-Ytterbium Waveguide Laser Mode-locked with a Semiconductor Saturable Absorber Mirror." IEEE. Photon. Technol. Lett., Forthcoming.

Joschko, M., P. Langlois, E. R. Thoen, E. M. Koontz, E. P. Ippen, and L. A. Kolodziejski, "Ultrafast Hot-Carrier dynamics in Semiconductor Saturable Absorber Mirrors." Appl. Phys. Lett., Forthcoming,

III. Enhanced Performance of Optical Sources in III-V Materials Using Photonic Crystals

Sponsors
National Science Foundation
DMR 94-00334 (OSP 67415)
Army Research Office
DAAG 55-98-1-0474 (OSP 67382)
Army Research Office
DAAG 55-98-1-0080 (OSP 66504)

Project Staff
Professor Leslie A. Kolodziejski, Professor John D. Joannopoulos, Professor Erich P. Ippen, Professor Henry I. Smith, Dr. Gale S. Petrich, Dr. Pierre R. Villeneuve, Dr. Shanhui Fan, Alexei Erchak, Steven G. Johnson and Daniel J. Ripin.

Keywords: Photonic Bandgap Structures, Waveguides, Microcavity, Light Emitting Diodes

This project represents the combined efforts of the research groups led by Professors John D. Joannopoulos, Leslie A. Kolodziejski, Erich P. Ippen, and Henry I. Smith. Prof. Joannopoulos' research group designs the structures and theoretically calculates the optical properties. Prof. Kolodziejski's group fabricates the various devices with embedded one- and two-dimensional photonic bandgap crystals using III-V compound semiconductor technologies. Prof. Smith's group provides the expertise in nanoscale fabrication. Finally, Prof. Ippen's research group optically characterizes the devices. The complexity of the design, fabrication and characterization of these structures necessitates a strong interaction between the various research groups.

III.A A Two-Dimensional Photonic Bandgap Light-Emitting Diode

A photonic bandgap (PBG) is the optical analog of an electronic bandgap in a semiconductor. A periodic variation in the dielectric constant forbids the propagation of photons with certain energies. Specifically, a two dimensional PBG inhibits the propagation of light within a certain range of frequencies in any direction in a plane. In this work, a two dimensional PBG is fabricated in the top cladding layer of an InGaP/InGaAs quantum well structure that emits at λ = 980 nm. The photonic crystal is designed such that the emission wavelength lies inside the photonic bandgap and hence does not couple to guided modes within the semiconductor. Coupling to the guided modes is a major source of loss in conventional light-emitting diodes (LED). In the structure being fabricated, this problem is greatly reduced and the amount of light radiated from the device is enhanced.

The two-dimensional PBG LED consists of an InGaAs active region with InGaP cladding layers, a low refractive index Al_xO_y spacer layer, and an Al_xO_y/GaAs distributed Bragg reflector (DBR) with a wide stop band. The fabrication of the 2D PBG LED utilizes gas source molecular beam epitaxy, direct-write electron beam lithography, reactive-ion etching, and oxidation processes. Figure 3a shows a schematic of the structure. The 2-D photonic crystal consists of a triangular lattice of holes etched within the upper InGaP cladding layer with a hole-to-hole spacing of 315 nm, and a hole diameter of 220 nm (figure 3b). To minimize

carrier recombination at the etched surfaces, the holes do not penetrate the InGaAs quantum well; however, the depth of the holes is sufficient to create a PBG (figure 3c). The active quantum well region lies on top of a DBR designed to reflect the 980 nm light; the spacer layer is used to minimize coupling to lateral guided modes in the DBR. Each 2-D PBG LED is a 12.5 μm x 12.5 μm region within the 50 μm x 50μm LED mesa (figure 3d).

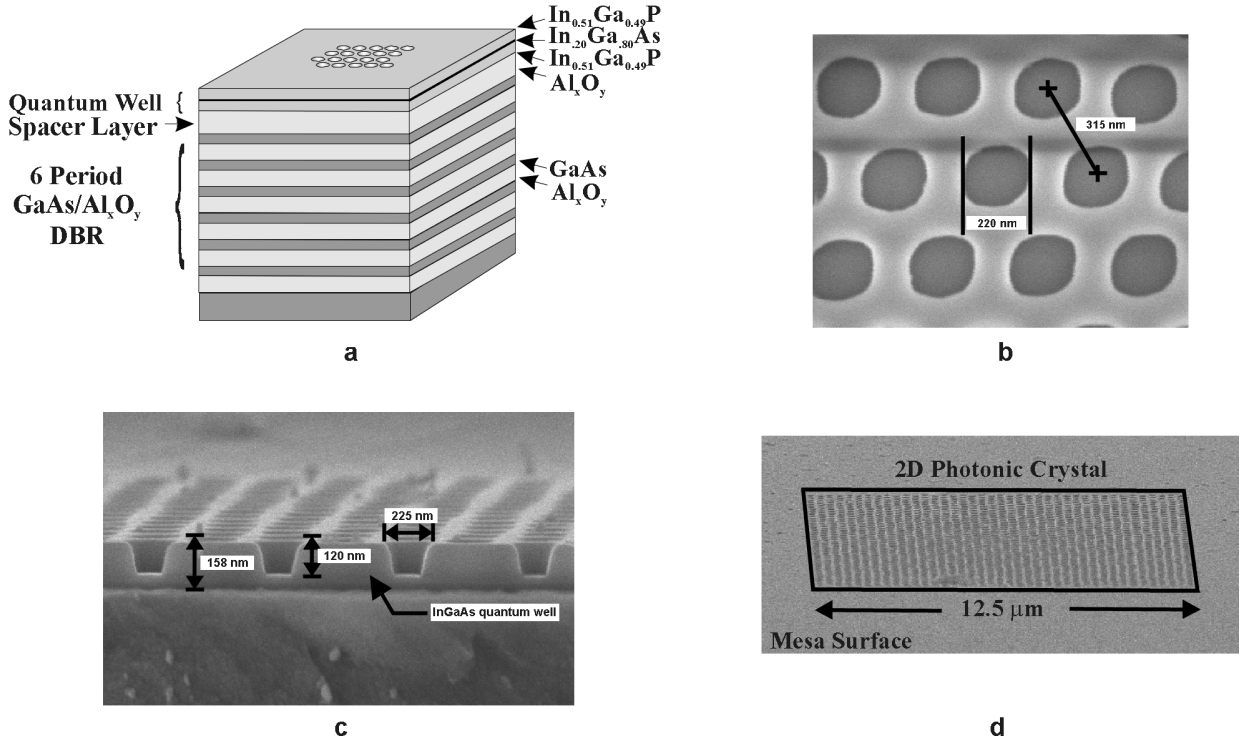

Figure 3) a) Schematic of 2-D PBG LED structure. The InGaP/InGaAs quantum well structure emits at λ = 980 nm. The active region is separated from the DBR by a low refractive index Al_xO_y separation layer. A triangular lattice of holes in the top layer of the device eliminates coupling of emitted light to planar guided modes. b) An SEM micrograph showing the dimensions of the triangular arrray of holes forming the photonic crystal. c) Cross-sectional view of 2-D PBG LED structure. The holes do not penetrate the InGaAs quantum well to avoid surface recombination. d) SEM micrograph of the 2D photonic crystal.

The device structure is grown using gas-source molecular beam epitaxy. The separation layer is initially grown as $Al_{0.98}Ga_{0.02}As$ and the DBR consists of AlAs and GaAs layers. A SiO_2 layer is deposited on the grown structure using plasma-enhanced chemical vapor deposition. The holes are defined in PMMA by direct-write electron-beam lithography. The electron beam writes a square pattern in the PMMA to represent each hole. The beam size, however, is larger than the step size for translating the electron beam. This leads to the desired circular pattern following development.

The PMMA is used as a mask in order to transfer the triangular pattern to the SiO_2 layer. This is accomplished by RIE using 15 seconds of CHF_3 plasma in between one-minute cool-down steps, during which the electrode is cooled with He gas flow. The purpose of the cool-down step is to prevent the flowing of the PMMA mask. The SiO_2 mask is subsequently used in the RIE of the holes into the upper InGaP cladding layer; the RIE step uses a CH_4/H_2 plasma in a 1:4 gas flow ratio. The mesas are next defined using

photolithography followed by RIE using a $BCl_3/SiCl_4$ plasma in a 3:2 gas ratio. The final step in the device fabrication is the wet thermal oxidation of the $Al_{0.98}Ga_{0.02}As$ separation layer and the AlAs DBR layers.

Room temperature photoluminescence (PL) spectroscopy is performed with a cw 810 nm $Ti:Al_2O_3$ pump laser, focused to a 6 μm diameter spot size on the sample. The pump is absorbed by the InGaAs quantum well layer, the GaAs substrate, and is reflected by the underlying DBR. The PL was measured both spectroscopically and spatially. A sample containing a number of LED mesas is translated in 1 μm step sizes to study the PL with spatial resolution. The PL spectra are shown in Figure 4 above a schematic of the line scan trajectory. The bottom trace shows the GaAs PL collected at 890 nm. The GaAs PL is observed in the spaces between the mesas. On the mesas, the DBRs prevent the pump light from exciting the GaAs substrate. The middle trace is the same line scan, now collecting light emitted by the quantum well at 980 nm. The PL signal increases on the mesa. The top trace shows a line scan at 980 nm through mesas containing PBG crystals. In addition to 50 μm wide features similar to the middle trace, narrow peaks of greater intensity are observed at the spatial position of the PBG crystal. An intensity enhancement of approximately 6-fold is observed from the 2-D PBG LED as compared to the LED region with no PBG crystal and is expected theoretically. Additional optical experiments and fabrication of new structures are underway to further verify the presence of the photonic bandgap effect.

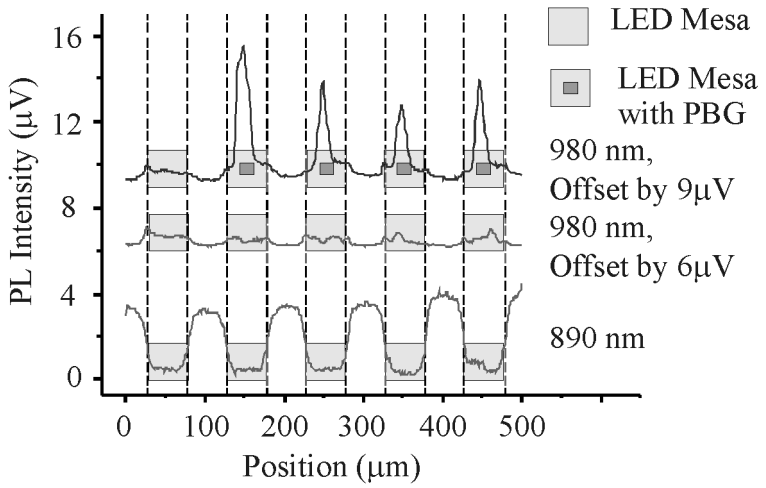

Figure 4) Spatially resolved photoluminescence (PL) is taken with the 2D PBG LED sample translated with respect to the pump beam. The position of the pump beam during each line scan is shown by the schematics below each trace. The bottom trace is collected at 890 nm, and is the PL from the GaAs substrate. The middle trace, collected at 980 nm, is the PL from the quantum well. The top trace is the PL from a line scan passing through one mesa without a PBG crystal, and four mesas with PBG crystals.

III.B A Photonic Bandgap Microcavity Laser Embedded in a Strip Waveguide

A one-dimensional photonic crystal is fabricated within a strip waveguide to provide strong optical confinement and a small modal volume on the order of a half-cubic wavelength. The microcavity is formed by a defect in the one-dimensional periodic photonic crystal. Optical confinement is achieved in the lateral and vertical directions by a high refractive index contrast. A high-efficiency, low-threshold, microcavity laser results with light output coupling to the strip waveguide. The structure is designed to be integratable with other optoelectronic devices.

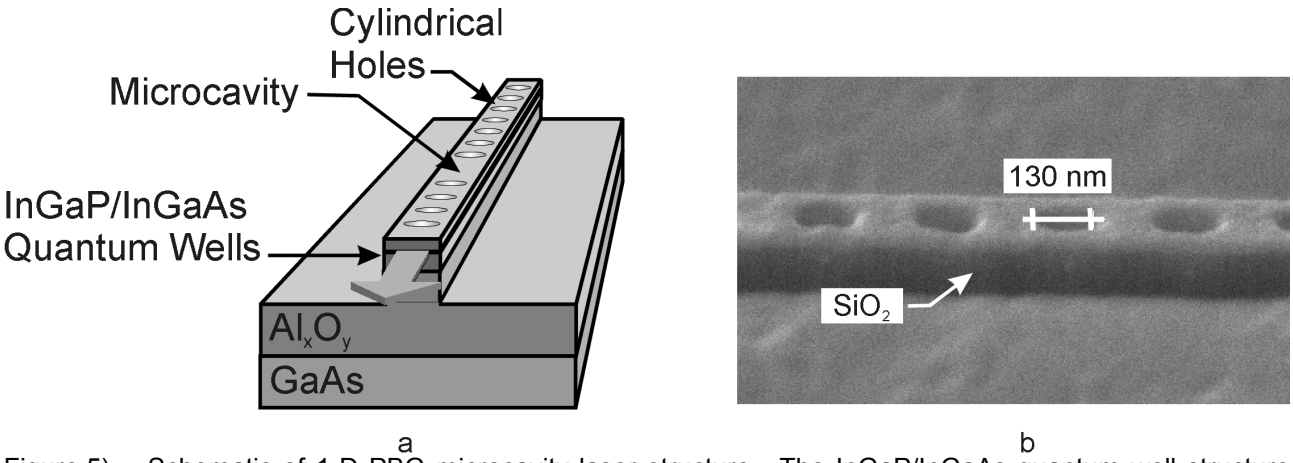

Figure 5) Schematic of 1-D PBG microcavity laser structure. The InGaP/InGaAs quantum well structure emits at λ=980 nm. The active region is separated from the GaAs substrate by a low refractive index Al_xO_y separation layer. The line of cylindrical holes forming the photonic crystal provide strong optical confinement along the waveguide while a high index contrast provides confinement in the lateral and vertical directions. b) An SEM micrograph showing an SiO_2 etch mask used in the RIE pattern transfer to the quantum well active region.

The one-dimensional PBG microcavity laser consists of an InGaP/InGaAs multiple quantum well active region emitting at λ=980 nm, on top of a low refractive index Al_xO_y spacer layer. Figure 5a shows a schematic of the structure. The 1D photonic crystal consists of a periodic array of holes etched within the active region with a hole-to-hole spacing of 256 nm and a hole diameter of 113 nm. The strip waveguide width is 320 nm and the waveguide depth is 112 nm. The length of the defect region is 426 nm. The active quantum well region lies on top of a low index spacer layer to separate the waveguide mode from the high index substrate. The laser output will occur on the side of the defect with the least number of holes.

The device structure is grown using gas-source molecular beam epitaxy. The separation layer is initially grown as $Al_{0.9}Ga_{0.1}As$ and graded up to higher Ga composition by dropping the Al cell temperature by 20°C and raising the Ga cell temperature by 20°C for 2 minutes. The composition is graded to stabilize the interface with the active region upon oxidation of the spacer layer. A SiO_2 layer is deposited on the grown structure using plasma-enhanced chemical vapor deposition. The holes and strip waveguide are defined in PMMA by direct-write electron-beam lithography. The pattern is then reversed using a nickel liftoff process. The pattern is transferred from the Ni to the SiO_2 by RIE with a CHF_3 plasma. The Ni mask is then removed using a wet Ni etchant. Figure 5b shows an SEM micrograph of a portion of a fabricated SiO_2 etch mask.

The SiO_2 mask will be used in the RIE of the holes into the InGaP/InGaAs active region with a CH_4/H_2 plasma in a 1:4 gas flow ratio. The CH_4/H_2 plasma etching slows at the $Al_{0.9}Ga_{0.1}As$ spacer layer. RIE of the spacer layer shall be accomplished using a $BCl_3/SiCl_4$ plasma in a 3:2 gas ratio. The SiO_2 mask will then be

removed by RIE with a CHF_3 plasma. The next step in the fabrication is the wet thermal oxidation of the $Al_{0.9}Ga_{0.1}As$ separation layer. Finally, the device will be cleaved on the output side of the laser to allow for device testing.

III. C Publications

Johnson, Steven G., Shanhui Fan, Pierre R. Villeneuve, J. D. Joannopoulos, and L. A. Kolodziejski, "Guided Modes in Photonic Crystal Slabs." Phys. Rev. B., 60(8): 5751-5758 (1999).

Ripin, D.J., Kuo-Yi Lim, G. S. Petrich, Pierre R. Villeneuve, Shanhui Fan, E. R. Thoen, J. D. Joannopoulos, E. P. Ippen, and L. A. Kolodziejski, "One-Dimensional Photonic Bandgap Microcavities for Strong Optical Confinement in GaAs and GaAs/Al_xO_y Semiconductor Waveguides." IEEE J. Light. Tech., 17(11): 2152-2160 (1999).

Lim, K.-Y., D. J. Ripin, G. S. Petrich, L. A. Kolodziejski, E. P. Ippen, M. Mondol, H. I. Smith, P. R. Villeneuve, S. Fan and J. D. Joannopoulos, "Photonic Bandgap Waveguide Microcavities: Monorails and Airbridges." J. Vac. Sci. Tech. B, 17(3): 1171-1174 (1999).

Lim, K.-Y., D. J. Ripin, G. S. Petrich, P. R. Villeneuve, S. Fan, J. D. Joannopoulos, E. P. Ippen, and L. A. Kolodziejski, "The role of the thermal oxide in GaAs-based photonic bandgap waveguide microcavities." Adv. Mater., 11(6): 501-505 (1999).

References

[1] H. A. Haus and Y. Lai, "Narrow-band distributed feedback reflector design," J. Lightwave Technol. 9(6): 754-760 (1991).

[2] H. A. Haus and Y. Lai, "Narrow-band optical channel-dropping filter," J. Lightwave Technol. 10(1): 57-62 (1992).

[3] J. N. Damask, "Practical design of side-coupled quarter-wave shifted distributed-Bragg resonant filters," J. Lightwave Technol. 14(5): 812-821 (1996).

[4] D. Rosenblatt, A. Sharon and A. A. Friesem "Resonant grating waveguide structures," IEEE J. Quantum Electron. 33(11): 2038-2059 (1997).

[5] J.N. Damask, private communication, (1997).

[6] B.- T. Lee, R. A. Logan and S. N. G. Chu, "Observation of growth patterns during atmospheric pressure metalorganic vapor phase epitaxy regrowth of InP around etched mesas," J. Crystal Growth 130: 287-294 (1993).

[7] R. Butendeich, M. Hurich and H. Heinecke, "Material localization at GaInAsP-ridge-structure selectively grown by MOMBE," J. Crystal Growth 195: 510-515 (1998).

[8] T. Matsui, K. Ohtsuka, H. Sugimoto, Y. Abe and T. Ohishi, "1.5μm GaInAsP/InP buried-heterostructure laser diode fabricated by reactive ion etching using a mixture of ethane and hydrogen," Appl. Phys. Lett. 56: 1641-1642 (1990).

[9] R. J. Simes, E. G. Goarin, C. Labourie, D. Bonnevie, A. Perales, D. Lesterlin and L. Goldstein "GSMBE growth on patterned substrates for optoelectronic devices," Proc. 4th Int. Conf. on InP and Related Materials (Piscataway, NJ: IEEE Publications, 1992).

[10] B.-T. Lee, R. A. Logan, R. F. Kalicek, Jr., A. M. Sergent, D. L. Coblentz, K. W. Wecht and T. Tanbun-Ek, "Fabrication of InGaAsP/InP buried heterostructure laser using reactive ion etching and metalorganic chemical vapor deposition, " IEEE Photon. Technol. Lett. 5: 279-281 (1993).

[11] B. Baur, H. Heinecke, M. Schier and N. Emeis, "Growth of GaInAs(P)/InP heterostructures on nonplanar substrates using MOMBE/CBE," J. Crystal Growth 127: 175-178 (1993).

[12] X. G. Xu, Ch. Giesen, R. Hövel, M. Heuken and K. Heime, "Surface morphology and growth rate variation of InP on patterned substrates using tertiarybutylphosphine," J. Crystal Growth 191: 341-346 (1998).

[13] E. L. Hu, C-H. Chen and D. L. Green, "Low-energy ion damage in semiconductors: A progress report," J. Vac. Sci. Technol. B 14: 3632-3636 (1996).

[14] S. Murad, M. Rahman, N. Johnson, S. Thoms, S. P. Beaumont and C. D. W. Wilkinson, "Dry etching damage in III-V semiconductors," J. Vac. Sci. Technol. B 14: 3658-3662 (1996).

[15] A. Izrael, D. Robein, and C. Vaudry, "Epitaxial overgrowth on nanometer InP wires processed by reactive ion etching," Microelectron. Eng. 13: 395-398 (1991).

[16] G. Biasiol and E. Kapon, "Mechanism of self-limiting epitaxial growth on nonplanar substrates," J. Crystal Growth 201/202: 62-66 (1999).

[17] S. L. Chuang, *Physics of Optoelectronic Devices,* (New York, New York: John Wiley and Sons, Inc, 1995).

[18] Q. Shen, S.W. Kycia, E.S. Tentarelli, W.J. Schaff, and L.F. Eastman, "X-ray diffraction study of size-dependent strain in quantum wire structures," Phys. Rev. B 54(23): 16381-16384 (1996).

[19] J. Shah, *Ultrafast Spectroscopy of Semiconductors and Semiconductor Nanostructures*, (Berlin, Springer-Verlag, 1996.)

[20] B.E. Bouma, G.J. Tearney, S.A. Boppart, M.R. Hee, M.B. Brezinski, and J.G. Fujimoto, "High-resolution optical coherence tomographic imaging using a mode-locked Ti:Al_2O_3 laser source," Opt. Lett. 20(13): 1486-1488 (1995).

[21] U. Keller, in *Nonlinear Optics in Semiconductors II*, eds. E. Garmire and A. Kost, (Boston, MA: Academic, 1999).

[22] B. C. Collings, J.B. Stark, S. Tsuda, W. H. Knox, J.E. Cunningham, W. Y. Jan, R. Pathak, and K. Bergman, "Saturable Bragg reflector self-starting passive mode locking of a Cr^{4+}:YAG laser pumped with a diode-pumped Nd:YVO_4 laser," Opt. Lett. 21(15): 1171-1173 (1996).

[23] S. Tsuda, W.H. Knox, and S. T. Cundiff, "High efficiency diode pumping of a saturable Bragg reflector-mode-locked Cr:LiSAF femtosecond laser," Appl. Phys. Lett. 69(11): 1538-1540 (1996).

[24] G.S. Gray and A.B. Grudinin, "Soliton fiber laser with a hybrid saturable absorber," Opt. Lett. 21(3): 207-209 (1996).

[25] Z. Zhang, K. Torizuka, T. Itatani, K. Kobayashi, T. Sugaya, and T. Nakagawa, "Femtosecond Cr:Forsterite laser with mode locking initiated by a quantum well saturable absorber," IEEE J. Quantum Electron. 33(11): 1975-1981 (1997).

[26] E.R. Thoen, E.M. Koontz, D.J. Jones, F.X. Kärtner, E.P. Ippen, L.A. Kolodziejski, and D. Barbier, "Suppression of instabilities and pulsewidth limitation by two-photon absorption in mode-locked lasers", in *Conference on Lasers and Electro-Optics, OSA Technical Digest* (Washington, DC: Optical Society of America, 1999).

[27] E.R. Thoen, E.M. Koontz, M. Joschko, P. Langlois, T.R. Schibli, F.X. Kärtner, E.P. Ippen, and L.A. Kolodziejski, "Two-photon absorption in semiconductor saturable absorber mirrors," Appl. Phys. Lett. 74: 3927-3929 (1999).

[28] P. Langlois, M. Joschko, E.R. Thoen, E.M. Koontz, F.X. Kärtner, E.P. Ippen, and L.A. Kolodziejski, "High fluence ultrafast dynamics of semiconductor saturable absorber mirrors", submitted to Appl. Phys. Lett.

[29] E.R. Thoen, E.M. Koontz, D.J. Jones, P. Langlois, F.X. Kärtner, E.P. Ippen, L.A. Kolodziejski, and D. Barbier, "Picosecond Pulses from an Er/Yb Waveguide Laser Passively Mode-locked with a Semiconductor Saturable Absorber Mirror", in *Conference on Lasers and Electro-Optics, OSA Technical Digest* (Washington, DC: Optical Society of America, 1999).

[30] E.R. Thoen, E.M. Koontz, D.J. Jones, D. Barbier, F.X. Kärtner, E.P. Ippen, and L.A. Kolodziejski, "Erbium-Ytterbium Waveguide Laser Mode-locked with a Semiconductor Saturable Absorber Mirror," IEEE Photon. Technol. Lett. Forthcoming.

[31] B.E.A. Saleh, M.C. Teich, *Fundamentals of Photonics*, (NewYork, New York: John Wiley and Sons, Inc., 1991).

[32] M.J. Adams, D.A.O. Davies, M.C. Tatham, and M.A. Fisher, "Nonlinearities in semiconductor laser amplifiers," Optical and Quantum Electronics 27: 1-13 (1995).

[33] R.J. Manning, A.D. Ellis, A.J. Poustie, and K.J. Blow, "Semiconductor laser amplifiers for ultrafast all-optical signal processing," J. Opt. Soc. Am. B 14(11): 3204-3216 (1997).

[34] *Quantum Well Lasers*, eds. P.S. Zory Jr., (Boston, MA: Academic Press, Inc., 1993).